Journal of Aeronautics, Astronautics and Aviation, Vol. 56, No. 1S, pp. 147 – 155 (2024)
DOI: https://doi.org/10.6125/JoAAA.202403_56(1S).07

Visualizing Partially Loosened Fastener through Frequency-Wavenumber Analysis of Ultrasonic Wavefield

Shi Yn Lee [1], Chen Ciang Chia [2 *], Fairuz Izzuddin Romli [1], Norkhairunnisa Mazlan [1], Jung-Ryul Lee [2], Mohammad Yazdi Harmin [1 **]

[1]*Department of Aerospace Engineering, Universiti Putra Malaysia, 43400 UPM Serdang, Selangor Darul Ehsan, Malaysia*
[2]*Department of Aerospace Engineering, KAIST, Daejeon 34141, Republic of Korea*

ABSTRACT

Aerospace thin-walled structures and alike are susceptible to various damages and flaws, including the loosening of fasteners, that must be non-destructively evaluated and repaired to avoid catastrophic failure. Guided ultrasonic wavefield has great potential to evaluate loosened fasteners, but state-of-the-art result processing methods are either not supporting direct visualisation of a loosened fastener or are unable to quantify the level of loosening. In this work, a more detailed analysis of the wavefield data was experimentally conducted in the frequency and wavenumber domains using wavenumber highpass and bandpass filters, as well as the wavenumber imaging algorithm. Six fasteners fixed at a simple aluminium plate were inspected, among which one was deliberately loosened from the nominal 100 lb-in to a few discrete levels to simulate a flaw. The imaging results revealed that a fastener loosened to 0, 20, 40, and 60 lb-in, respectively, could be distinctively visualised but marginally discernible when loosened to 80 lb-in. Further work is being conducted to improve the detection sensitivity and properly quantify the results.

Keywords: Non-destructive testing and evaluation (NDT&E); Structural health monitoring (SHM); Structural inspection; Laser ultrasound imaging; Lamb waves

I. INTRODUCTION

Advances in aerospace structure has immensely led into a strong and lightweight structure which nowadays can be idealised through an approach of innovative structural design concept [1-4], thin-wall design principles, as well as in composite material technology [5-7]. Nevertheless, the design of such structure including its manufacturing and certification process are growing increasingly complicated, necessitating advancement in structural inspection in order to ensure its integrity. Therefore, a non-destructive testing (NDT) technology is among the approach that can be adopted. Generally, NDT is a collection of inspection techniques commonly used in various industries, like aerospace, automotive, power, marine, and so on, for the detection of damage or inspection of object quality without causing any damage to the object being inspected [8]. A wide range of NDT techniques can be applied to various structures, depending on the materials, and expected type of damage [9,10]. In recent decades, NDT has been included more and more extensively in the aircraft maintenance program to ensure flight safety as a primary factor in getting an airworthiness certificate [11,12]. In Malaysia, NDT holds vital importance in aircraft maintenance, as it is a prerequisite for obtaining the Airworthiness Certificate prior to commencing flight operations, particularly for civil aircraft registered under the Civil Aviation Authority of Malaysia (CAAM) [13,14].

Manuscript received, September 29, 2023, final revision, November 3, 2023
* To whom correspondence should be addressed, E-mail: chiacc@kaist.ac.kr
** To whom correspondence should be addressed, E-mail: and myazdi@upm.edu.my

Aerospace structures are susceptible to many types of damage, including fatigue cracks, impact delamination, and corrosion. Relatively less well-known to the public is that catastrophic accidents could also happen due to a missing or loosened fastener. Fastener loosening can result from explicit factors such as improper installation and the use of incorrect or damaged fasteners. Additionally, implicit factors, like variation in operational loads [15], can lead to self-loosening. For example, in 2011, a Robinson R44 Astro crashed onto the runway of Cessnock Aerodrome Australia and killed two people due to a loosened bolt [16]. In 2015, an untightened nut of oxygen tubing caused a $62.4 million loss to the U.S. Air Force [17]. So far, the detection of fastener loosening relies heavily on the onboard instrumentation of all fasteners, such as optical fibre bending sensor [18] and shear-wave electromagnetic acoustic transducer [19]. The major drawback is the need to install many permanent sensors and data acquisition systems on board the aircraft, causing unnecessary mass increment.

Guided ultrasonic waves propagation imaging (G-UPI) [20] that can detect many types of damage [21-25] without needing any permanently bonded sensor or onboard instrumentation has attracted some research groups' attention. The Lamb waves, which is a type of guided ultrasonic waves, is typically used due to their capability of insonifying the entire thickness of aircraft skin for a large distance, enabling efficient detection of hidden defects nondestructively [26]. Tola et al. [27] exploited the polar directionality of the wavefield data in the wavenumber-frequency domain to isolate backscattering from a target fastener. The backscattered wavefield was then carefully gated (i.e., windowed or demarcated) in the time- and space-domain to calculate the cumulated wave energy (CWE). The CWE for all fasteners was plotted as a bar graph. The graph showed an inversed correlation of CWE with the tightness level of the fasteners. However, this method requires ad hoc or case-dependent calculations for further confirmation. Moreover, the result was not given in image form but as a bar graph.

Haynes et al. [28] also tried detecting loosened fasteners using the G-UPI technique. They proposed a damage-index algorithm for detecting bolt loosening in a simple lap joint specimen. This method is based on the ratio of root-mean-square energy transmitted through the joint, the root-mean-square energy at each bolt head, and the symmetricity level of the wavefield transmitted across the lap joint. They successfully showed a significant difference between the fully tightened bolts and the fully loosened ones. However, the resolution of the algorithm was insufficient to differentiate a partially loosened bolt.

Gooda Sahib et al. [29] processed the wavefield data using a result processing method known as Ultrasonic Spectral Imaging (USI) in combination with a customised contrast maximisation algorithm. They demonstrated the visualisation of a fully loosened fastener in a simple lap joint specimen. This method allows the detection of a loosened fastener from an image; thus, it is significantly more intuitive and easier to use. The disadvantage of this method is that it can only indicate the fully loosened fastener, but not those partially loosened.

In summary, conventional methods could differentiate either a fully loosened fastener through image visualisation or differentiate a partially loosened fastener without any image visualisation after extensive ad hoc processing. In this study, a wavenumber-frequency domain analysis of the wavefield data is proposed to facilitate the detection of loosened fasteners based on image visualisation while having sufficient resolution to differentiate partially loosened fasteners quantitatively. The data acquisition system and specimen used are described in Section 2. The domain conversion and analysis methods are described as well. The results are discussed in Section 3, and lastly, the conclusions and future works are given in Section 4.

II. SETUP AND METHODOLOGY

This section describes the methodological design of current study. The experimental investigation was performed using a simple plate specimen with six (6) fasteners. The specimen's design and technique used to control the loosening level of the fasteners were described in sub-section 2.1. The experimental setup for wavefield measurement was described in sub-section 2.2. Lastly, the result processing methods employed in this study were explained in sub-section 2.3.

2.1. Specimen and Fastener Loosening

A simple 500×500×2 mm^3 aluminium plate was used as a specimen in this study. Six 6.7±0.3 mm diameter holes were drilled at 100 mm from the plate centre in a polar symmetric arrangement, in which fasteners (stainless-steel M6×16 mm bolts and nuts) were fixed, as shown in Figure 1.

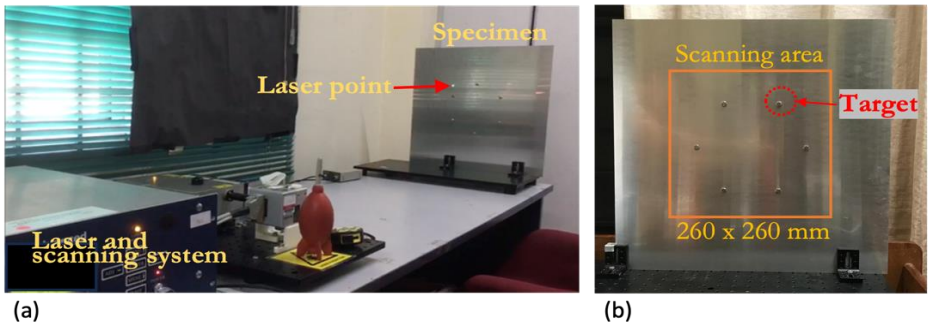

Figure 1 Inspection setup (a) Overview (b) Specimen plate with six sets of fasteners fixed in a polar symmetric arrangement. The target fastener was located at the top-right corner.

The fasteners were tightened to a nominal 100 lb-in using a torque wrench. The target fastener, located at the top-right corner, was tightened to various torque levels before wavefield measurement, according to the sequence listed in Table 1.

Table 1 Torque Level of Target Fastener

Inspection Sequence	1	2	3	4	5	6
Torque level	0 lb-in (0 Nm)	20 lb-in (2.26 Nm)	40 lb-in (4.52 Nm)	60 lb-in (6.78 Nm)	80 lb-in (9.04 Nm)	100 lb-in (11.30 Nm)

2.2. Wavefield Measurement

A G-UPI system [20] with a laser for ultrasound generation and a fixed-position amplifier-integrated PZT (lead zirconate titanate) sensor was used for wavefield measurement, as shown in Figure 2. The laser was a diode-pumped solid-state Q-switched pulsed laser with a wavelength of 532 nm, beam diameter of about 4 mm, a pulse width of about 40 ns, pulse energy of about 1.5 mJ, and pulse repetition frequency of 50 Hz. Rectilinear grid-scanning was realised using a galvano-motorized laser mirror scanner, with a scanning interval of 0.5 mm in both the horizontal x and vertical y directions. The imaging region of interest (ROI) was a 260 by 260 mm^2 region at the centre of the specimen plate, which enclosed all fasteners. The sensor was bonded at the plate centre using cyanoacrylate adhesive on the opposite side of the laser-scanning surface. The ultrasound wave generated at each scanning grid point was converted by the sensor into an analogue electrical signal. All signals were converted into digital signals by an 8-bit oscilloscope using a 5 MHz sampling frequency and 500 sample points. The ultrasound generation measurement was performed consecutively for all scanning grid points, one after another, until the signals from all scanning grid points were saved as a three-dimensional (3D) space-time wavefield data denoted as $v[x, y, t]$, where x, y and t represents the horizontal x-direction, vertical y-direction, and time index, respectively.

2.3. Wavefield Analysis

The acquired wavefield data $v[x, y, t]$ were first analysed in the original space-time domain, and then analysed in the wavenumber-frequency domain and the wavenumber-time domain. Domain transformations were performed because sparse information carried by a wavefield is coupled in the space-time domain but can be compressed into respective modes for information decoupling in the wavenumber and/or frequency domain, thereby enabling more processing options [30-32]. Descriptions of respective analysis methods are given in the following sub-sections.

2.3.1. Space-Time Domain

Analysis in the space-time domain was performed as a standard procedure to validate the data quality. In this context, the acquired wavefield data were synthesised into an animated wavefield propagation video following the steps described in [33]. The gist of this processing is to display the t^{th} time slices of the 3D data $v[x, y, t]$ as two-dimensional (2D) images $v_t[x, y]$ at a video-refresh rate consecutively for t = 0, 1, 2, …, T-1, where T represents the total time samples of the wavefield data. Using this processing method, the wavefield at any of its propagation instances could hence be visualised as a concentric wavefield propagating outward from the sensing position, and wavefield interactions with the fasteners could also be understood to facilitate further advanced or detailed analysis.

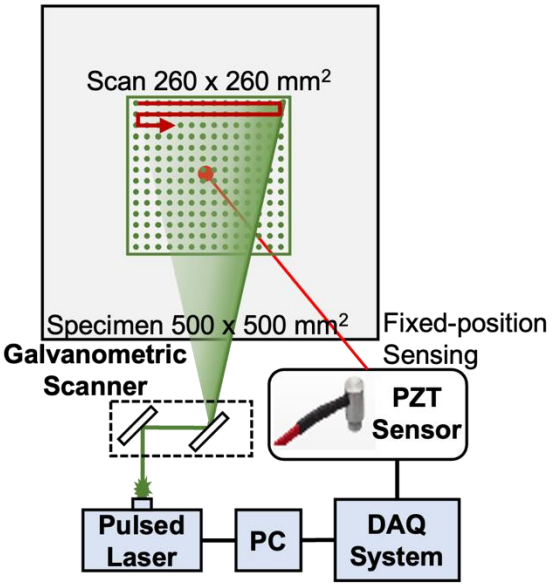

Figure 2 Schematic diagram of the G-UPI system featuring a scanning laser for ultrasound generation and a fixed-position sensor for ultrasound measurement. PZT: lead zirconate titanate; PC: personal computer; DAQ: data acquisition

2.3.2. Wavenumber-Frequency Domain

Wavenumber-frequency domain analysis was performed by converting the space-time data $v[x, y, t]$ as the wavenumber-frequency data $V[\kappa_x, \kappa_y, f]$ using 3D Fourier transformation (FT) [32,34], as shown in Equation (1). Throughout this paper, the symbol f represents the

frequency, and the symbol κ represents the wavenumber; thus κ_x and κ_y represents the x-direction and y-direction wavenumber, respectively. The data were filtered in the frequency domain and wavenumber domain to determine a wavenumber that can represent the local wavenumber value of the specimen based on the wavenumber imaging algorithm described in [35].

$$v[x,y,t] \xrightarrow{3D\ FT} V[\kappa_x,\kappa_y,f] \quad (1)$$

2.3.3. Wavenumber-Time Domain

Wavenumber-time domain analysis was performed by converting the space-time data $v[x,y,t]$ as wavenumber-time data $V[\kappa_x,\kappa_y,t]$ using 2D FT, as shown in Equation (2). Then, the binary mode filter window described in [36] was modified into a wavenumber highpass window $\widetilde{W}_{HP}[\kappa_x,\kappa_y]$ and a wavenumber bandpass window $\widetilde{W}_{BP}[\kappa_x,\kappa_y]$ by changing the wavenumber bandwidth to suit the analysis of fastener loosening. Filtering is performed according to Equation (3). Result visualisation was performed by plotting the wavenumber-filtered data as a spectral energy map (SEM) [36,37].

$$v[x,y,t] \xrightarrow{2D\ FT} V[\kappa_x,\kappa_y,t] \quad (2)$$

$$V \cdot \widetilde{W}[\kappa_x,\kappa_y] \quad (3)$$

III. RESULTS AND DISCUSSION

The wavefield data were first analysed in the space-time domain using a wavefield propagation video. The video and its snapshots showed a concentric wavefield propagating outward from the centre of inspection ROI, as shown in Figure 3.

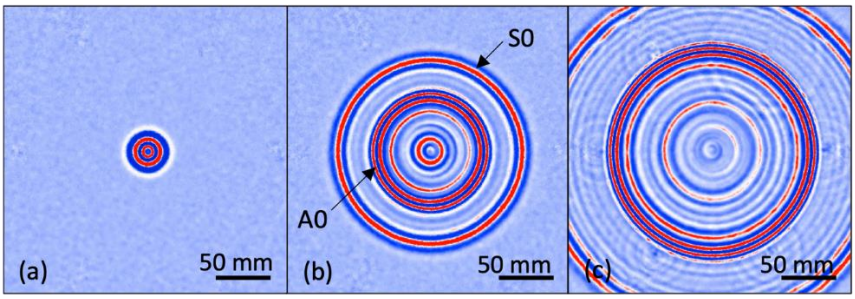

Figure 3 Snapshots of wavefield propagation video at (a) 6 μs, (b) 19 μs, and (c) 32 μs of propagation instance, showing concentric wavefield emanating outward from the centre.

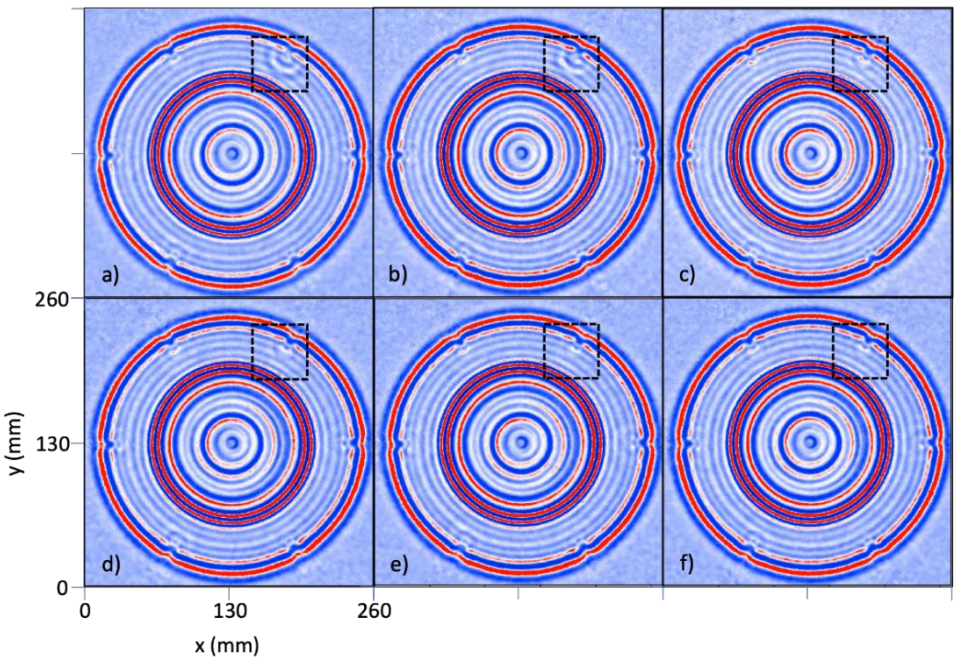

Figure 4 Wavefield snapshots showing the reflections of S0 mode when the target fastener had a torque level of (a) 0, (b) 20, (c) 40, (d) 60, (e) 80, and (f) 100 lb-in.

The fundamental symmetric mode (S0 mode) and antisymmetric mode (A0 mode) of the wavefield can be seen at the 19 μs of propagation, as shown in Figure 3(b). The S0 mode propagated further away from the central wavefield source due to its higher group velocity than the A0 mode [34]. At later propagation instances, the wave modes propagated further and may interact with the fasteners, as shown in Figure 3(c). Figure 4 showed the reflected wavefield (reflection) of S0 mode at 25 μs of propagation when the target fastener had different torque levels. Close examination of Figure 4(a) showed that the reflection from the target fastener (target reflection), which was fully loosened at 0 lb-in, was stronger than the reflections from other fasteners that were fully tightened at 100 lb-in. A similar condition can be observed when the target fastener was tightened to 20, 40, and 60 lb-in, as shown in Figure 4(b) to (d), respectively. Enlarged views of the dashed-boxed regions are given in Figure 5.

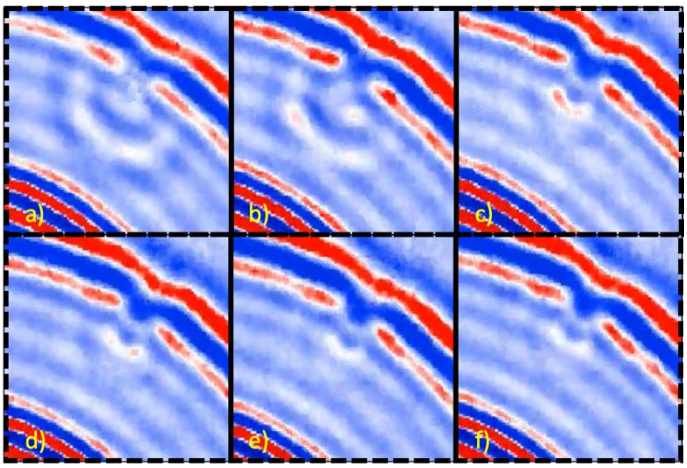

Figure 5 Enlarged views of target reflections at (a) 0, (b) 20, (c) 40, (d) 60, and (e) 80 lb-in, together with (f) the nominal reflection at 100 lb-in.

It is obvious that the target reflections at 0 and 20 lb-in, as shown in Figure 5(a) and (b), are different from the reflection at 100 lb-in (nominal reflection), as shown in Figure 5(f). The target reflections at 40 and 60 lb-in, as shown in Figure 5(c) and (d), can be seen different from the nominal reflection only with careful examination. Target reflection at 80 lb-in, as shown in Figure 5(e), cannot be differentiated from the nominal reflection, thus indicating undetectable loosening. Most probably, the subtle target reflection was overshadowed by the strong nominal reflection, or there was destructive interference between the reflection due to a phase mismatch, which requires further investigation.

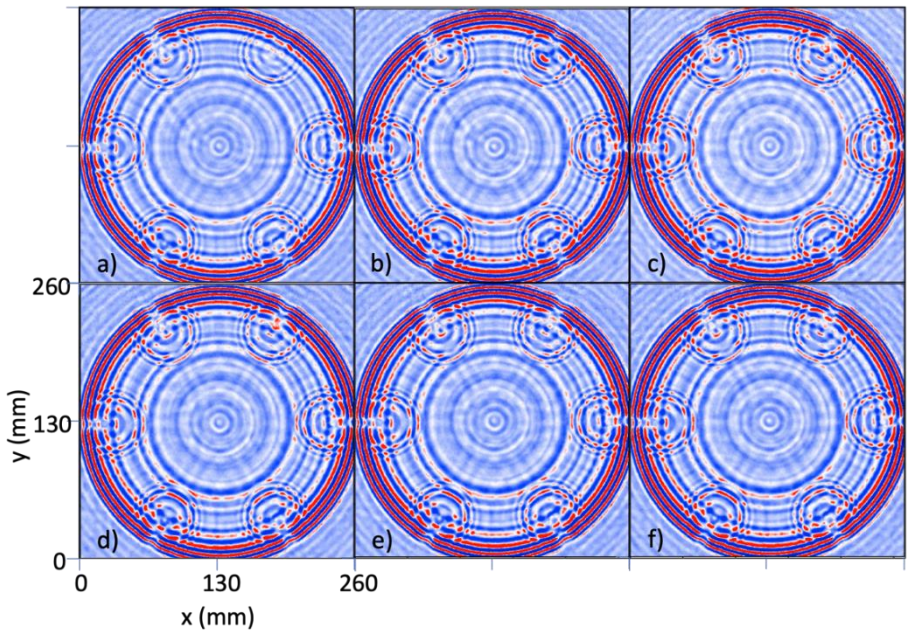

Figure 6 Wavefield snapshots showing the reflections of A0 mode when the target fastener had a torque level of (a) 0, (b) 20, (c) 40, (d) 60, (e) 80, and (f) 100 lb-in.

The reflections of A0 mode were inspected, as shown in the 43 μs snapshots given in Figure 6. Unfortunately, the target reflections at different torque levels are indifferent. This condition was unexpected because the A0 mode is known to be more sensitive to structural damage and flaw [38-40]. The reason behind this contradiction is subject to further investigation.

To improve the accuracy of analysis, the space-time domain wavefield data was analysed in the wavenumber and frequency domains. The results were visualized as a wavenumber map, a spectral energy map (SEM) with a 0 m^{-1} wavenumber highpass, and a SEM with a 40-90 m^{-1} wavenumber bandpass, as shown in Figure 7(a) to (c), respectively. Similar to previous results, enlarged views of the results at the target fastener are needed. The enlarged views of the wavenumber maps are given in Figure 8. Figure 8(a) shows that the fully loosened fastener exhibited a higher wavenumber value, indicated as a yellowish-orange region in the map. Some yellow regions can also be seen for the target fastener loosened to 20 lb-in and 80 lb-in, but this has no consistent trend and cannot be correlated to the loosening level.

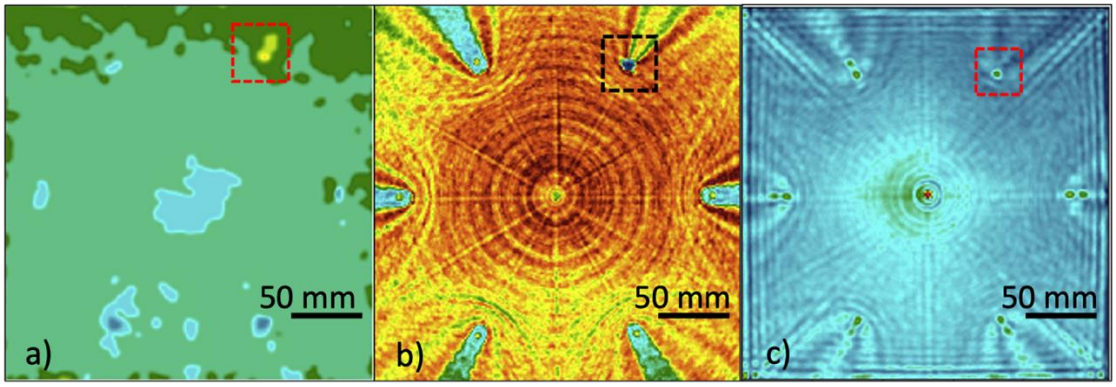

Figure 7 Wavefield data processed as (a) wavenumber map, (b) SEM with a 0 m-1 wavenumber highpass, and (c) SEM with a 40-90 m-1 wavenumber bandpass.

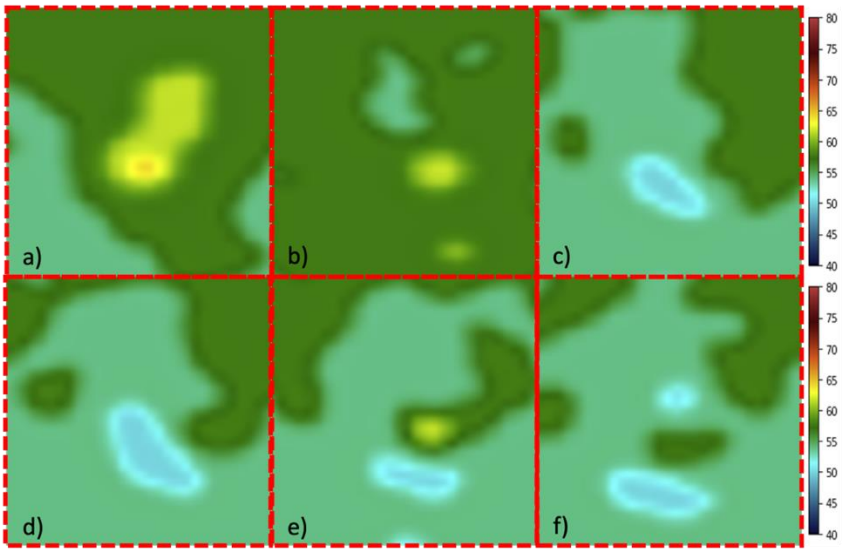

Figure 8 Wavenumber map zoom-in at the target fastener corresponds to torque level of (a) 0, (b) 20, (c) 40, (d) 60, (e) 80, and (f) 100 lb-in. Unit of colour scale = m-1

The zoomed-in views of SEM after wavenumber highpass processing at 0 m^{-1} are given in Figure 9 with a normalized colour scale. Figure 9(a) shows that the fully loosened fastener could be easily identified due to the significant difference in appearance compared to the other cases. With careful observation, a yellow dot can be spotted at the centre of the fastener for cases of higher torque levels, starting from 40 lb-in. The yellow dot does not exist for the 20 lb-in cases, suggesting that the 20 lb-in case is also distinguishable. An interesting finding from this analysis is the higher sensitivity of the wavenumber highpass at 0 m^{-1}, as opposed to other higher ranges of wavenumber. Somehow this finding is consistent with the space-time domain analysis, in which the S0 mode with a lower wavenumber was found more sensitive to the loosening of the target fastener.

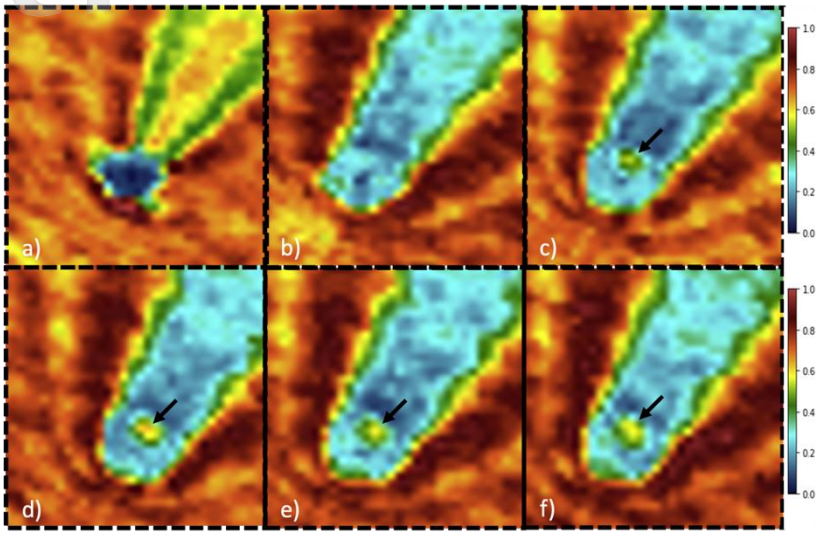

Figure 9 Zoom-in views of SEM after wavenumber highpass processing at 0 m-1 for target fastener at torque levels of (a) 0, (b) 20, (c) 40, (d) 60, (e) 80, and (f) 100 lb-in.

In order to achieve a higher resolution, a wavenumber bandpass at 40-90 m^{-1}, which had a much narrower bandwidth compared to the broadband 0 m^{-1} highpass, was adopted. The bandpassed data were processed as SEM, as shown in Figure 10 using a normalized colour scale. The energy level and distribution of the fully-loosened target fastener are obviously different from the other cases, as shown in Figure 10(a), with only one primary energy 'blob' in green. With a gradual increment of fastener torque, a secondary energy 'blob' gradually appears next to the primary 'blob'. At 20 lb-in, the secondary 'blob' started to appear. It started to separate from the primary 'blob' at 40 lb-in. It grew larger to its full size at 60 lb-in, similar to the size of secondary 'blob' at 80 and 100 lb-in. The secondary 'blob' fully detached from the primary 'blob' at 80 lb-in. These images and chronology showed that the loosening level of the fasteners could be visualised and distinguished directly using the ultrasound wavefield imaging.

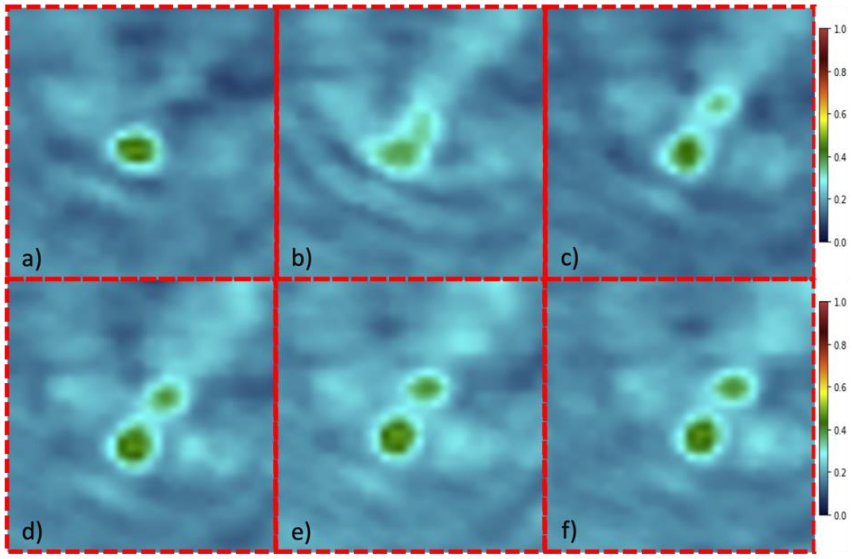

Figure 10 Zoom-in views of SEM after wavenumber bandpass processing at 40-90 m-1 for target fastener at torque levels of (a) 0, (b) 20, (c) 40, (d) 60, (e) 80, and (f) 100 lb-in.

IV. CONCLUSIONS

Loosened fasteners in critical engineering structures such as aircraft and bridges could cause catastrophic failure. Conventional data processing methods for guided ultrasonic wavefield imaging could be used to visualise fully loosened fasteners or differentiate the level of loosening without any direct visualisation. Still, they

cannot achieve both at the same time. A structured analysis of the wavefield data in the original space-time domain, and in the Fourier-transformed wavenumber and frequency domains was performed in this study to harness the full potential of wavefield imaging. A simple aluminium plate with six fasteners tightened to a nominal 100 lb-in was used for experimental investigation. Wavefield data were acquired when the target fastener was deliberately partially tightened to 0, 20, 40, 60, and 80 lb-in. Analysis of the wavefield datasets in the space-time domain suggested that the S0 mode has higher sensitivity than the A0 mode. This situation was unexpected because the A0 mode is well documented in the literature to be more sensitive to structural damages and flaws due to its shorter wavelength. Nevertheless, further analysis of the wavefield datasets in the wavenumber and frequency domains confirmed that the fastener loosening is more visible at lower wavenumber ranges, i.e., wavenumber bandpass 40-90 m^{-1} used in this study. The results also showed distinguishable energy levels and distributions for the target fastener at different levels of loosening. In conclusion, suitable wavenumber and frequency filtering could be used to visualise and discern fasteners at various levels of loosening. Further work is being conducted to quantify the results properly, so that a clear correlation between the level of loosening and a suitable ultrasound parameter can be established. Possible reasons for higher S0 sensitivity, as well as the influences of plate thickness and lap-joint fastening, are also being investigated.

ACKNOWLEDGMENTS

This research was supported and funded by Universiti Putra Malaysia through the Industrial Research Grant Scheme of Tan Sri Syed Azman Syed Ibrahim's Endowment Fund (Account vote number: 6338201-10801).

REFERENCES

[1] Dawood SDS, Harmin MY, "Structural Responses of a Conceptual Microsatellite Structure Incorporating Perforation Patterns to Dynamic Launch Loads," *Aerospace*, Vol. 9, No. 8, 2022, pp. 448-473.

[2] Dawood SDS, Harmin MY, Harithuddin ASM, Chia CC, Rafie ASM, "Computational Study of Mass Reduction of a Conceptual Microsatellite Structural Subassembly Utilizing Metal Perforations," *Journal of Aeronautics, Astronautics and Aviation*, Vol. 53, 2021, pp. 57-66.

[3] Chan YN, Rafie ASM, Harmin MY, "Investigation of Modal Strain Energy for Varying Ribs Orientation Concept of Untapered Wing Box Model," *Journal of Aeronautics, Astronautics and Aviation*, Vol. 54, No. 3, 2022, pp. 307-13.

[4] Chan YN, Harmin MY, Othman MS, "Parametric study of varying ribs orientation and sweep angle of un-tapered wing box model," *International Journal of Engineering & Technology*, Vol. 7, No. 4, 2018, pp. 155-159.

[5] Mohammed I, Talib ARA, "Strength Behaviour of Silica Aerogel/Thermoset Polymer with Reinforced Fibre-metal Laminate Composites for Aero-engine Firewall," *Journal of Aeronautics, Astronautics and Aviation*, Vol. 52, No. 1, 2020, pp. 15-23.

[6] Chok EYL, Majid DLAA, Harmin MY, "Effect of low velocity impact damage on the natural frequency of composite plates," *IOP Conference Series: Materials Science and Engineering*, Vol. 270, 2017, 012025.

[7] Mohammed I, Talib ARA, "Experimental Investigation of Metal- Laminates with Aerogel in High-Temperature Application," *Journal of Aeronautics, Astronautics and Aviation*, Vol. 53, 2021, pp. 121-127.

[8] Moore PO, Workman GL, Nondestructive Testing Overview, Ohio, USA: The American Society for Nondestructive Testing, Vol. 10, 2012.

[9] Dwivedi SK, Vishwakarma M, Soni Prof A, "Advances and Researches on Non Destructive Testing: A Review," *Materials Today: Proceedings*, Vol. 5, 2018, pp. 3690-3698.

[10] Gholizadeh S, "A review of non-destructive testing methods of composite materials," *Procedia Structural Integrity*, Vol. 1, 2016, pp. 50-57.

[11] National Research Council, Nondestructive Evaluation, Washington, DC, USA, The National Academies Press,Chap. 8 1996, pp. 67-70.

[12] De Florio F, Airworthiness, Oxford, UK, Butterworth-Heinemann, Chap. 2, 2016, pp. 5-6.

[13] CAAM, "Civil Aviation Guidance Material-8601: Maintenance Organisation Approval," CAGM 8601-CAAM Part 145 Issue 01/Rev 00, Civil Aviation Authority of Malaysia, Malaysia, Nov. 2022.

[14] CAAM, "Civil Aviation Directive-8501: Mandatory Continuing Airworthiness Information-Airworthiness Directives," CAD 8501-MCAI Issue 01/Rev 00, Civil Aviation Authority of Malaysia, Malaysia, Feb. 2022.

[15] Carone S, Pappalettera G, Casavola C, De Carolis S, Soria L, "A Support Vector Machine-Based Approach for Bolt Loosening Monitoring in Industrial Customized Vehicles," *Sensors*, Vol. 23, No. 11, 2023, pp.5345-5361.

[16] The Australia Transport Safety Bureau, "Loss of Control - Robinson Helicopter R44 Astro VH-HFH, Cessnock Aerodrome, NSW, on 4 February 2011," AO-2011-016, Australian Capital Territory, Australia, Apr. 2012.

[17] Evans WM, "United States Air Force Aircraft Accident Investigation Board Report," RC-135V, T/N 64-14848, Air Force Air Combat Command, Joint Base Langley-Eustis, Virginia, Aug. 2015.

[18] Shin HJ, Lee JR, Park CY, "Loosening Monitoring of Bolted Joints Using Optical Fiber Bending Sensor for Aircraft Lug Assembly," *Applied Mechanics and Materials*, Vol. 225, 2012, pp. 540-545.

[19] Hirao M, Ogi H, Yasui H, "Contactless measurement of bolt axial stress using a shear-wave electromagnetic acoustic transducer," *NDT & E International*, Vol. 34, 2001, pp. 179-183.

[20] Chia CC, Lee SY, Harmin MY, Choi Y, Lee J-R, "Guided Ultrasonic Waves Propagation Imaging: A Review," *Measurement Science and Technology*, Vol. 34, 2023, 052001.

[21] Gan CS, Tan LY, Chia CC, Mustapha F, Lee J-R. "Nondestructive detection of incipient thermal damage in glass fiber reinforced epoxy composite using the ultrasonic propagation imaging," *Functional Composites and Structures*, Vol. 1, 2019, 025006.

[22] Chia CC, Gan CS, Gomes C, Mazlan N, Gomes A. "Lightning Damages in Glass Fiber-Epoxy Composite Material used for Aerospace Applications," 34th International Conference on Lightning Protection (ICLP*)* 2018 34th International Conference on Lightning Protection (ICLP), 2018, pp. 1-4.

[23] Chia CC, Jang SG, Lee J-R, Yoon DJ, "Structural damage identification based on laser ultrasonic propagation imaging technology," Optical Measurement Systems for Industrial Inspection VI, Vol. 7389, 2009, 73891S.

[24] Chia CC, Lee J-R, Park CY, "Radome health management based on synthesized impact detection, laser ultrasonic spectral imaging, and wavelet-transformed ultrasonic propagation imaging methods," *Composites Part B: Engineering*, Vol. 43, 2012, pp. 2898-2906.

[25] Chia CC, Jeong H-M, Lee J-R, Park G, "Composite aircraft debonding visualization by laser ultrasonic scanning excitation and integrated piezoelectric sensing," *Structural Control and Health Monitoring*, Vol. 19, 2012, pp. 605-620.

[26] Su Z, Ye L, Identification of Damage Using Lamb Waves: From Fundamentals to Applications, Berline/Heidelberg, Germany, Springer, Vol. 48, 2009, Chap. 5, pp. 143-186.

[27] Tola KD, Lee C, Park J, Kim J-W, Park S, "Bolt looseness detection based on ultrasonic wavefield energy analysis using an Nd:YAG pulsed laser scanning system," *Structural Control and Health Monitoring*, Vol. 27, No. 9, 2020, e2590.

[28] Haynes C, Yeager M, Todd M, Lee J-R, "Monitoring bolt torque levels through signal processing of full-field ultrasonic data," Health monitoring of structural and biological systems 2014 Conference Proceedings. Vol. 9064, 2014, pp. 906428–1-906428–9.

[29] Gooda Sahib MI, Leong SJ, Chia CC, Mustapha F, "Detection of fastener loosening in simple lap joint based on ultrasonic wavefield imaging," *IOP Conference Series: Materials Science and Engineering*, Vol. 270, 2017, 012035.

[30] Ruzzene M, "Frequency-Wavenumber Domain Filtering for Improved Damage Visualization," AIP Conference, Vol. 894, 2006, pp. 1556-1563.

[31] Michaels TE, Michaels JE, Ruzzene M. "Frequency–wavenumber domain analysis of guided wavefields," *Ultrasonics*, Vol. 5, 2011, pp. 452-466.

[32] Ma Z, Yu L, Chao YJ, Lam P-S, Sindelar RL, Duncan AJ, Truong T-T, Verst C, Sun P-K, Campbell A. "Nondestructive Evaluation of Stress Corrosion Cracking in a Welded Steel Plate Using Guided Ultrasonic Waves," *Journal of Nondestructive Evaluation, Diagnostics and Prognostics of Engineering Systems*, Vol. 5, No. 3, 2022, 031003.

[33] Chia CC, Lee JR, Park J-S, Yun C-Y, Kim JH, "New design and algorithm for an ultrasonic propagation imaging system," Defektoskopie 2008, 38th International Conference, 2008, pp. 63-70.

[34] Zhang H, Sun J, Rui X, Liu S, "Delamination damage imaging method of CFRP composite laminate plates based on the sensitive guided wave mode," *Composite Structures*, Vol. 306, 2023, 116571.

[35] Flynn EB, Chong SY, Jarmer GJ, Lee J-R, "Structural imaging through local wavenumber estimation of guided waves," *NDT & E International*, Vol. 59, 2013, pp. 1-10.

[36] Shahrim MAA, Chia CC, Ramli HR, Harmin MY, Lee J-R, "Adaptive Mode Filter for Lamb Wavefield in the Wavenumber-Time Domain Based on Wavenumber Response Function," *Aerospace*, Vol. 10, No. 4, 2023, pp. 347-367.

[37] Shahrim MAA, Lee SY, Lee J-R, Harmin MY, Chia CC, "Visualization of Water Ingress in Aluminium Honeycomb Sandwich Panel through Mode Isolation of Lamb Wavefield," *Journal of Aerospace Society Malaysia*, Vol. 1, 2023, pp. 9-18.

[38] Truong T C, Lee J-R, "Thickness reconstruction of nuclear power plant pipes with flow-accelerated corrosion damage using laser ultrasonic wavenumber imaging," *Structural Health Monitoring*, Vol. 17, 2017, pp. 255-265.

[39] Wandowski T, Mindykowski D, Kudela P, Radzienski M, "Analysis of Air-Coupled Transducer-Based Elastic Waves Generation in CFRP Plates," *Sensors*, Vol. 21, No. 21, 2021, pp. 7134-7167.

[40] Zheng S, Luo Y, Xu C, Xu G, "A Review of Laser Ultrasonic Lamb Wave Damage Detection Methods for Thin-Walled Structures," *Sensors*, Vol. 23, No. 6, 2023, pp. 3183-3209.